Research article

Paleogeography of the southwestern Ordos Basin and exhumation history of the Liupan Shan area

Fangbin Liu [a,b,*], Min Wang [a]

[a] School of Geography and Tourism, Qilu Normal University, Ji'nan, 250200, China
[b] Key Laboratory of Western China's Environmental Systems, Ministry of Education, College of Earth and Environmental Sciences, Lanzhou University, Lanzhou, 730000, China

ARTICLE INFO

ABSTRACT

The Liupan Shan, situated on the southwestern Ordos Basin, underwent Cenozoic uplift caused by the India-Asia collision and subsequent northeastward tectonic movements. The strata in this region record both the paleogeography of the southwestern Ordos Basin and the uplift history of the Tibetan Plateau. However, past studies have rarely analyzed the strata comprehensively, resulting in overlooked information within them. We present the first detrital zircon (U-Th)/He (ZHe) data from the Lower Cretaceous deposits of the Liupan Shan and the Upper Miocene red clay of Chaona, constraining a maximum burial depth of less than 6–7 km at 60 Ma for the Liupan area. By integrating zircon U-Pb ages, paleocurrent data, and sedimentary facies, we found a primary ZHe age peak (~210 Ma) indicating that the Lower Cretaceous deposits were sourced from the Qinling Orogenic Belt, while the red clay was likely originated from the Liupan Shan. Although the Chaona strata are not preserved in the Liupan Shan, our results suggest that the Miocene Chaona section is crucial for understanding the Late Cenozoic uplift of the Liupan Shan. The distinct stratigraphic ages and source areas reflect the complex depositional and tectonic history of the region. Thermal modeling results revealed three stages of tectonic events (Late Cretaceous, Late Paleocene-Early Eocene, and Late Cenozoic), which are linked to plate interaction. Our findings offer new insights into the long-term tectonic evolution of the Tibetan Plateau.

1. Introduction

The Mesozoic Ordos Basin, situated in the western part of the North China Craton, represents a large-scale intracontinental non-marine basin [1,2]. The development of Ordos Basin involved intense tectonic activities [3], making it widely recognized as an excellent example for studying the Mesozoic intraplate and deformation sedimentation in Asia. Previous studies regarding the paleogeographic reconstruction of the Mesozoic Ordos Basin have primarily focused on the Triassic [4–10] and Jurassic strata [5, 11–13]. However, few studies have addressed the Cretaceous period, and detailed paleogeographic analysis (e.g., provenance) for this period remain lacking. The Liupan Shan lies near the southwestern boundary of the Ordos Basin, but its Cenozoic uplift resulted from the India-Asia collision and the associated northeastward propagation of deformation [14–19]. The Cretaceous strata in the Liupan Shan area have a broad distribution, which not only record the paleogeographic evolution of southwestern Ordos Basin, but also reflect

---

the uplift/exhumation history and the underlying dynamic mechanisms.

Recently, several studies have focused on the Liupan Shan [14,17–24]. For example, Zheng et al. [14] investigated the geological evolution of the NE Tibetan Plateau using apatite fission track method. They identified a period of rapid cooling and exhumation around 8 Ma, associated with tectonic activity along the Liupan Shan thrust fault. It indicates that the NE Tibetan Plateau experienced simultaneous outward growth rather than sequential expansion. Subsequently, Lin et al. [17] summarized a cooling phase by fission track and magnetostratigraphy in the Sikouzi section, to the east of the Liupan Shan, dating to an initial time at 9.5 Ma. By contrast, this finding highlighted the relationship between these tectonic events and broader climatic and environmental changes, underscoring the interconnected nature of geological processes and environmental conditions. The rapid cooling event in the Late Miocene, revealed by fission track data, coincides with tectonic stress field evolution, sedimentary facies and rates changes observed in the stratigraphic record during corresponding time periods [19,21]. Furthermore, our previous research on fault geometry and kinematics confirmed that the Late Cenozoic uplift and exhumation of the Liupan Shan resulted from thrusting on the Liupan Shan thrust fault, with an average long-term slip rate of 0.54 km/Myr [23]. However, the details of sedimentary filling and tectonic evolution of the Liupan Shan before Cenozoic have not yet to be established. Fortunately, detrital zircon geochronology can play a key role in tracing sediment sources in orogenic systems [25,26], quantifying the basin burial and exhumation process [27–29], and tracking the source-to-sink evolution of sedimentary basins [30–32].

Here, we report some new detrital zircon (U-Th)/He thermochronological ages (ZHe) from the Lower Cretaceous sedimentary strata and the Upper Miocene red clay in the Liupan Shan and the southwestern Ordos Basin (Chaona), respectively. Integrating thermal modeling with existing low-temperature thermochronology data, we establish more robust constraints on the burial/exhumation histories and paleogeography of the Liupan Shan and the southwestern Ordos Basin since Mesozoic. These findings elucidate the long-term tectonic evolution and developmental processes of the NE Tibetan Plateau.

2. Geological setting

The Liupan Shan lies at the northeastern margin of the Tibetan Plateau, with an average elevation of ~2000 m, connecting the stable Ordos Block to the east and Alxa Block to the north, while the Qilian Shan and Qinling orogenic belts stand at the west and south, respectively [17,19,23] (Fig. 1). As the important boundary of the Tibetan Plateau, the evolution of the Liupan Shan can significantly influence tectonic deformation and dynamic mechanisms on the Tibetan Plateau. Previous studies demonstrated that the Liupan Shan underwent multistage orogeny, including the Early Paleozoic, Indosinian, Yanshan, and Himalayan [33]. During the Mesozoic, the study area and its adjacent region underwent a transition to an intraplate setting [3], being a part of the Ordos Basin. In the Early to Middle Jurassic, north-south directional extension dominated the tectonics of the western margin of the Ordos Basin, leading to the formation of lacustrine coal-bearing shales in the Liupan Shan [34–36]. In contrast, this extensional regime shifted in the Late Jurassic to east-west compression, creating fold-thrust structures and initiating mild uplift and erosion in the Liupan Shan area [34–36]. In the Early Cretaceous, the tectonic landscape evolved with the Ordos Block undergoing an anticlockwise rotation due to the northwestward subduction of the Pacific Plate. This significant movement resulted in the formation of large-scale grabens, such as the Liupan
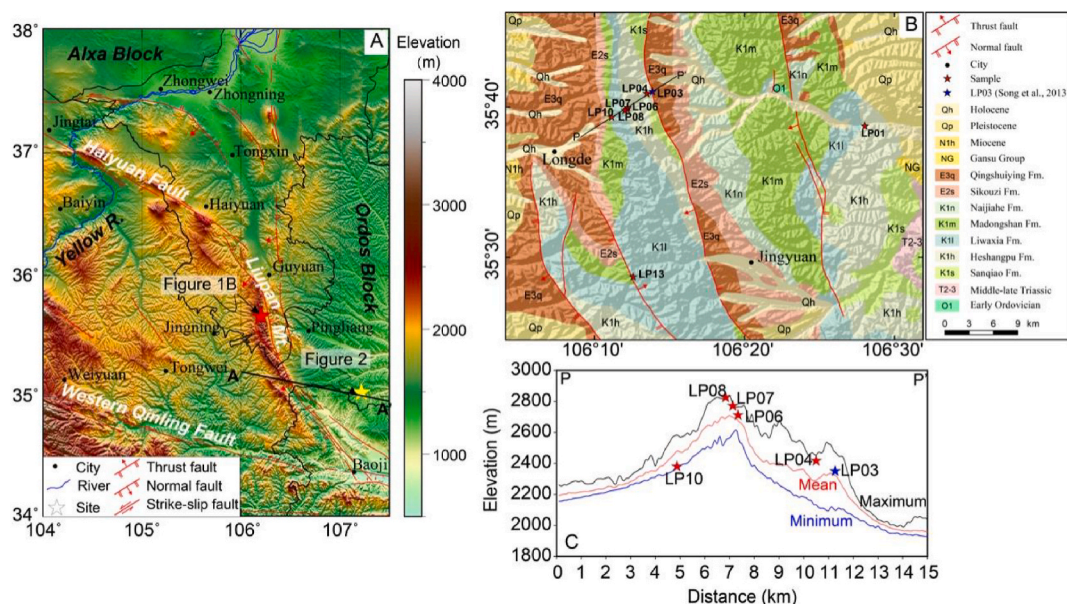

Fig. 1. (A) Topographic map of the Liupan Shan area with major structures and sites. The red star is the Liupan Shan area and the yellow star is the Chaona section. Black solid line (A–A′) is a section shown in Fig. 2. (B) Simplified geological map of the study area. (C) Topographic swath profile calculated using a 2-km window along section line P–P′ in (B).

Fault-Depression [35]. These grabens were filled with approximately 3000–4000 m thickness of fluvial-lacustrine clastic strata around Early Cretaceous [14,23,37]. In the late Early to Late Cretaceous, further compression in the northwest-southeast direction caused tectonic inversion in the Liupan Shan, highlighted by uplift and erosion along the Haiyuan-Liupan Fault [21]. The Cenozoic era was characterized by intense northeast-southwest and nearly east-west compressive stresses that led to pronounced folding and thrusting in the Liupan Shan, extending northeastward along several major faults due to the expansion of the Tibetan Plateau [14,22]. Multiple collision phases between the Indian and Eurasian plates elevated the Himalayas and triggered phased uplifts of the northeastern plateau margins around 60-50 Ma, 30 Ma, and 10 Ma, significantly shaping the region's geologic framework [23,38].

The Lower Cretaceous strata, defined as the Liupan Shan Group, are the main sedimentary units and are widely distributed in the Liupan Shan area [14,23,37] (Fig. 1). From bottom (old) to the top (young), the Lower Cretaceous strata are divided into five lithological units, including the Sanqiao Formation (K_1s), Heshangpu Formation (K_1h), Liwaxia Formation (K_1l), Madongshan Formation (K_1m), and Naijiahe Formation (K_1n) [22]. The Sanqiao Formation (129.6–128.6 Ma), primarily comprising conglomerate, breccia and pebbly coarse sandstone, suggests typical piedmont facies sedimentation. The Heshangpu Formation (128.6–125.3 Ma), a braided fluvial deposit, is mainly distributed in the east of the watershed in the middle of the Liupan Shan, showing a north-south zonal distribution. The formation reaches about 560 m thickness and comprises purplish-red coarse sandstone and mudstone, indicative of a relatively dry and hot climate. The Liwaxia Formation (125.3–118.3 Ma) is interpreted as shallow lacustrine environment, predominantly consisting of light blue and grey mudstone, grey sandstone, mudstone, and marl. Its thickness reaches up to 700 m. The Madongshan Formation (118.3–109.6 Ma) is mainly composed of mudstone, shale, and limestone, with ~400 m thickness. The Naijiahe Formation (109.6–102 Ma) is generally dominated by the mudstone, shale and limestone with gypsum [22,37,39].

The Chaona section is situated in the southwestern Ordos Block, with a GPS of 35°02′N and 107°13′E, at the eastern margin of the Liupan Shan (Figs. 1 and 2A). The loess-red clay sequence is well developed in this section, encompassing about 300 m thickness with upper layer of 175 m loess-paleosol and lower layer of 125 m Late Tertiary red clay [19]. Among while, the red clay sequence is divided into five units with thicknesses from top to bottom as follows: 21 m, 24 m, 25 m, 30 m and 28 m, ranging from ~2.6 to 8 Ma based on paleomagnetic dating [19]. The base of red clay (Unit V) lies unconformity atop the Lower Cretaceous strata (Fig. 2B).

3. Methods

3.1. Sampling strategy

We collected seven rock samples from Lower Cretaceous strata of the Liupan Shan (five sample from a vertical section; Fig. 1). A
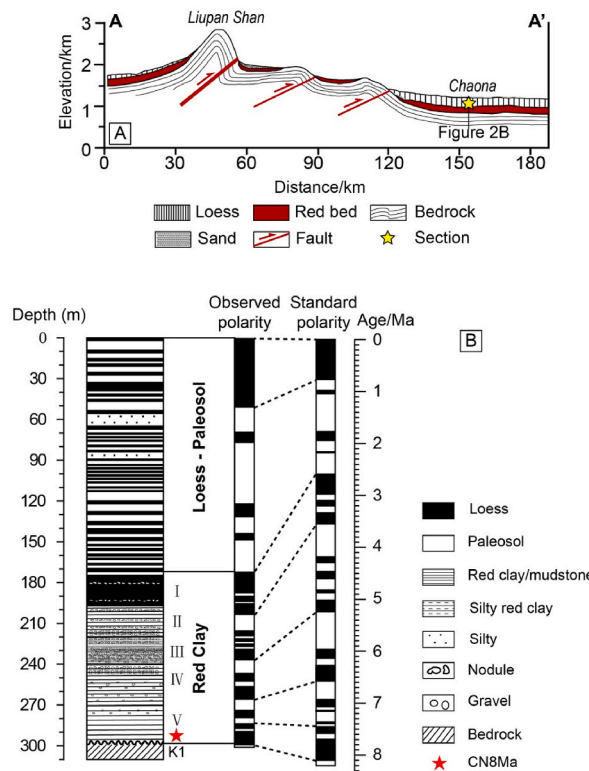

Fig. 2. (A) Late Cenozoic geological cross section of the Liupan Shan. (B) Stratigraphy and magnetostratigraphy of the loess-red clay sequence in the Chaona section at the east of the Liupan Shan. Revised from Song et al. [19].

previous study suggested that the bottom unit of red clay sequence, corresponding to ~8 Ma depositional ages, might be sourced from the Liupan Shan [31]. Consequently, one detrital sample was collected from the base of red clay to test the hypothesis (Fig. 2). Detailed sample information for the Liupan Shan and Chaona section is provided in Table 1 and Fig. 1.

3.2. ZHe dating method

The ZHe system reaches closure at temperatures ranging from 180 to 200 °C [40], significantly higher than those of apatite in the same system. Consequently, it offers constraints on the cooling and exhumation histories of the shallow crust at depths of ~6–7 km, with a typical geothermal gradient of 30 °C/km [23,41]. The ZHe dating technology primarily relies on the production of α particles through the series decay of parent isotopes ^{238}U, ^{235}U, and ^{232}Th, leading to the accumulation of ^{4}He. All the zircon samples were analyzed at the Isotope Geochemistry Laboratory of the University of Kansas. The experimental procedures followed the protocols of Wolfe and Stockli [41]. Initially, all samples were crushed, sieved, and separated using electromagnetic and heavy liquid methods. Following the routine mineral separation of zircon, grains were handpicked based on similar morphology, clarity, and size. Each grain underwent morphometric analysis to measure length and width, allowing for calculation of the alpha ejection correction factor (Ft) [42]. Single zircon aliquots wrapped in Pt were laser-heated with a 20 W Nd-YAG laser at 1300 °C for 10 min, followed by repeated reheating to ensure over 99 % degassing. The extracted gas was spiked with a ^{3}He tracer, cryogenically purified, and analyzed via isotope dilution using a quadrupole noble gas mass spectrometer. After He extraction, zircon grains were retrieved, unwrapped from Pt tubing, and subjected to a pressure vessel digestion procedure. This included spiking with enriched ^{230}Th and ^{235}U, followed by two-stage dissolution: (1) HF-HNO$_3$ mixture for 72 h at 225 °C, and (2) 6 N HCl for 12 h at 200 °C. Parent nuclide concentrations were measured via isotope dilution on a VG PQII quadrupole ICP-MS, comparing the spike to a gravimetric 1 ppb standard solution. Finally, the ZHe ages were determined using standard Ft corrections.

3.3. Thermal modeling

Although the apparent ages may not be directly connected with any particular geological event [43], the apparent ages, track length and Dpar values can play a key role in the thermal and exhumation history modeling of rock samples [44–46]. In the study, we performed inverse modeling for eight samples using QTQt software [47] to present the thermal history of source region and analyze the maximum burial depth/temperature of post-deposition, utilizing our new ZHe ages and published apatite fission track (AFT) data [48]. The QTQt software, known for its popularity and user-friendly interface, serves as a visual thermal history modeling tool. It determines the optimal time-temperature (*t*-T) path from thermochronological ages for multiple or single sample(s) with known altitudinal relationships, utilizing the Bayesian transdimensional Markov chain Monte Carlo (MCMC) inversion approach [47].

In addition, constraint boxes used for inversion modeling include stratigraphic ages with current average surface temperature (10 ± 10 °C) [23]. Meanwhile, the paleo-geothermal gradient is set to a broad range of 30 ± 30 °C/km, reflecting the current average geothermal gradient (20–25 °C/km) [23]. The final thermal history model underwent 100,000 iterations post-exploratory runs, with the first 50,000 iterations used for burn-in and the latter 50,000 considered as accepted models. Conducting exploratory runs with a higher number of iterations did not notably impact the model results.

4. Results

4.1. Detrital ZHe dating of the Liupan Shan

Seven detrital samples from the Lower Cretaceous (K$_1$h, K$_1$l) were analyzed for ZHe dating (Fig. 1; Table 1). All the single grains yield ZHe ages ranging from 621.2 ± 49.7 to 44.1 ± 2.6 Ma (Table 2). The age-elevation plot presents that all ZHe ages are not significantly changed with the elevation and much older than the corresponding sedimentary stratigraphic ages except LP06-1. This indicates that the samples were partial reset and buried below ~6–7 km depth (assuming the geothermal gradient of 30 °C/km) [23, 41](Fig. 3A). Consequently, the ZHe ages are interpreted as the detrital materials from source regions, documenting exhumation histories prior to deposition. Furthermore, we present the probability density function (PDF) plot and kernel density estimate (KDE) for all grains to better visualize the data spread [49]. As demonstrated in the plot (Fig. 3B), the majority of the data (17 out of 21 samples) range from 140 to 255 Ma, with a distinct peak at ~210 ± 10 Ma. The younger age (LP06-1) is considered anomalous due to the high

Table 1
Sample information of the Liupan Shan and Chana section.

Sample	Strata	Latitude	Longitude	Elevation (m)
LP01	K$_1$h	35°38′45.0″	106°28′01.0″	1605
LP04	K$_1$h	35°40′54.6″	106°13′29.2″	2418
LP06	K$_1$h	35°39′59.1″	106°12′12.6″	2713
LP07	K$_1$h	35°39′52.5″	106°12′10.1″	2773
LP08	K$_1$h	35°39′48.6″	106°12′02.0″	2828
LP10	K$_1$l	35°39′20.5″	106°11′08.2″	2382
LP13	K$_1$l	35°28′43.0″	106°12′34.0″	2529
CN8Ma	Red clay	35°02′	107°13′	/

Table 2
Zircon (U-Th)/He data in the Liupan Shan and Chaona section.

Sample	ESR (µm)	Mass (µg)	Ft	eU (ppm)	U (ppm)	Th (ppm)	He (nmol/g)	Raw age (Ma)	Corrected age (Ma)	± σ
Liupan Shan										
LP01-1	42.08	2.95	0.73	411.2	396.7	62.9	203.5	91.0	124.6	7.5
LP01-2	63.54	9.64	0.81	50.9	44.5	27.7	45.7	163.6	201.7	12.1
LP01-3	40.93	3.03	0.72	160.5	149.6	47.5	118.8	135.4	187.9	11.3
LP04-1	46.64	4.07	0.75	131.4	119.3	52.6	97.2	135.3	180.3	10.8
LP04-2	42.43	3.46	0.73	137.3	130.2	30.5	125.7	167.2	228.6	13.7
LP04-3	44.54	3.93	0.74	216.7	207.0	41.7	153.1	129.5	174.1	10.4
LP06-1	34.44	1.60	0.67	993.2	919.0	321.7	159.7	29.7	44.1	2.6
LP06-2	34.63	1.72	0.68	241.5	231.8	42.4	202.1	153.0	225.3	13.5
LP06-3	40.22	3.01	0.71	205.2	174.7	132.5	185.3	164.6	231.6	13.9
LP07-1	51.87	6.95	0.78	206.2	197.8	36.5	176.8	156.7	201.6	12.1
LP07-2	56.53	7.39	0.79	200.6	183.4	74.7	279.5	252.1	318.6	19.1
LP07-3	52.24	7.20	0.77	498.6	438.6	260.6	472.3	172.6	223.1	13.4
LP08-1	48.05	4.79	0.76	232.1	219.5	54.6	155.5	122.8	161.6	9.7
LP08-2	54.04	6.15	0.78	221.3	204.0	75.0	186.4	153.9	196.5	11.8
LP08-3	48.95	4.70	0.76	270.0	247.8	96.4	159.9	108.6	142.6	8.6
LP10-1	38.86	2.38	0.71	63.6	61.9	7.6	42.0	121.2	170.3	13.6
LP10-2	39.02	2.45	0.71	231.4	212.1	83.8	197.2	155.6	220.0	17.6
LP10-3	41.88	2.93	0.73	111.7	102.6	39.5	102.5	167.4	230.8	18.5
LP13-1	60.34	8.85	0.80	37.7	33.0	20.3	106.4	498.0	621.2	49.7
LP13-2	55.76	7.05	0.79	103.5	89.1	62.6	114.3	200.5	255.2	20.4
LP13-3	65.39	11.07	0.81	115.3	97.4	78.0	102.8	162.5	199.4	15.9
Chaona Red Clay										
CN8Ma-1	37.86	2.19	0.69	201.4	172.8	124.2	154.6	140.2	201.8	12.1
CN8Ma-2	39.25	2.42	0.70	256.9	215.2	180.8	245.2	173.8	247.1	14.8
CN8Ma-3	44.55	4.18	0.74	196.3	181.8	62.8	230.1	212.9	287.4	17.2
CN8Ma-4	52.04	6.01	0.77	174.9	143.8	134.8	168.9	175.7	228.2	13.7
CN8Ma-5	42.57	3.89	0.72	131.0	100.2	133.6	109.9	152.9	212.0	12.7
CN8Ma-6	31.90	1.38	0.64	265.1	225.2	173.4	305.3	209.0	324.3	19.5
CN8Ma-7	24.12	0.63	0.55	252.7	227.0	111.3	142.4	103.4	186.5	11.2
CN8Ma-8	35.60	1.96	0.68	173.8	152.8	91.4	130.6	137.3	202.2	12.1
CN8Ma-9	30.12	1.11	0.63	175.3	156.3	82.4	127.2	132.7	210.7	12.6
CN8Ma-10	28.06	0.90	0.60	151.7	125.2	115.4	189.3	226.0	375.9	22.6
CN8Ma-11	36.71	1.90	0.69	248.0	214.8	144.4	342.9	250.0	364.0	21.8
CN8Ma-12	42.31	2.95	0.73	287.8	255.3	141.1	333.6	210.5	290.0	17.4
CN8Ma-13	33.94	1.70	0.67	790.6	715.7	325.4	550.0	127.3	190.7	11.4
CN8Ma-14	42.98	3.29	0.73	141.9	120.7	92.2	138.9	178.1	244.9	14.7
CN8Ma-15	35.59	1.89	0.68	182.4	154.0	123.2	160.6	160.5	237.2	14.2
CN8Ma-16	40.99	2.76	0.72	167.6	149.3	79.9	177.1	192.2	267.7	16.1
CN8Ma-17	29.78	1.10	0.63	5.7	5.1	2.8	118.5	1235.8	1974.5	118.5
CN8Ma-18	24.86	0.66	0.56	464.3	409.1	239.5	384.3	151.1	268.2	16.1
CN8Ma-19	29.36	1.08	0.63	150.5	140.9	41.6	50.8	62.2	99.2	6.0
CN8Ma-20	35.97	1.95	0.68	142.6	127.3	66.4	148.8	189.9	278.0	16.7
CN8Ma-21	41.26	2.74	0.72	108.9	99.4	41.2	90.9	152.5	211.4	12.7
CN8Ma-22	30.35	1.12	0.63	87.9	80.0	34.3	90.8	188.1	296.7	17.8
CN8Ma-23	36.91	2.03	0.68	263.7	208.0	241.7	210.8	145.8	213.1	12.8

ESR: Equivalent sphere radius.

eU concentration or He loss resulting from metamictization, attributed to its small size (Table 2).

4.2. Detrital ZHe dating of the chaona section

We collected one sample named CN8Ma from the lowermost strata of the loess-red clay sequence and obtained ages for 23 grains (Fig. 3C). According to the age distribution, most of dates (18 out of 23) fall within a narrow range of 190–300 Ma. The age plot indicates a significant age peak at ~210 Ma (Fig. 3D), similar to that in the Liupan Shan area (Fig. 3B).

4.3. Inverse thermal history modeling

The *t*-T path predicted for sample LP01 indicates continuous cooling prior to deposition, followed by reheating from the depositional age (K$_1$h) up to ~60 Ma, reaching a peak temperature of 70 °C (expected model), before cooling to surface (Fig. 4A). The maximum temperature implies that LP01 did not undergo completely annealing.

The inverse thermal modeling output for sample LP03, derived from the Sanqiao Formation (K$_1$s), is solely based on AFT data [48]. The modeling illuminates a two-stage thermal history, the first heating starting from surface through ~100 °C at the Paleocene,
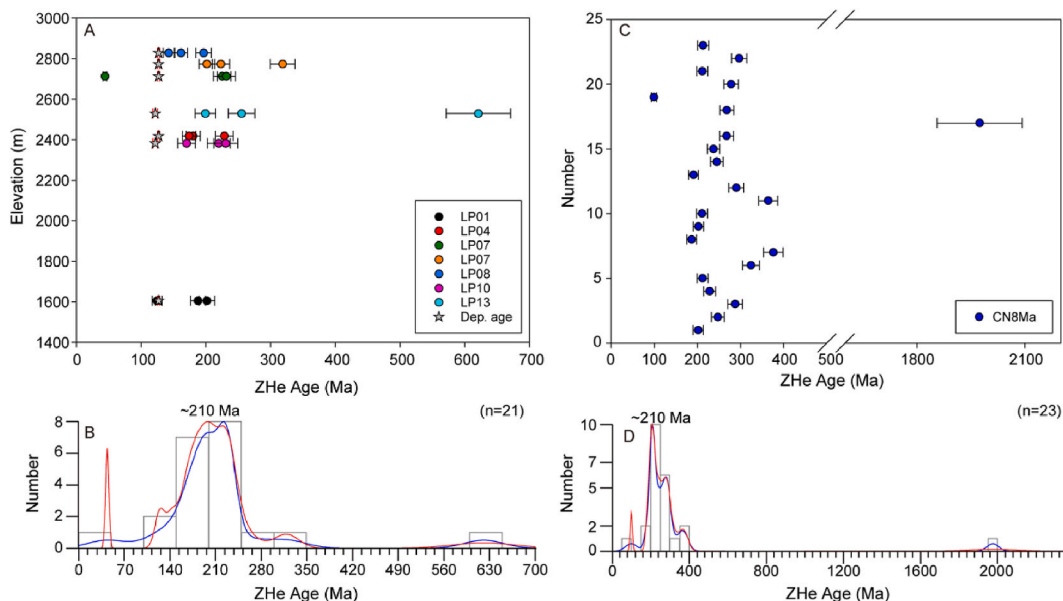
Fig. 3. Comparison of the Liupan Shan and lowermost red clay (CN8Ma) samples. (A) ZHe age-elevation plot for the Liupan Shan. The grey star is the deposition age of corresponding strata. (B) Probability density plots (red line) and kernel density estimate (blue line) of ZHe ages for the Liupan Shan. Bandwidth = 50 Ma. (C) ZHe 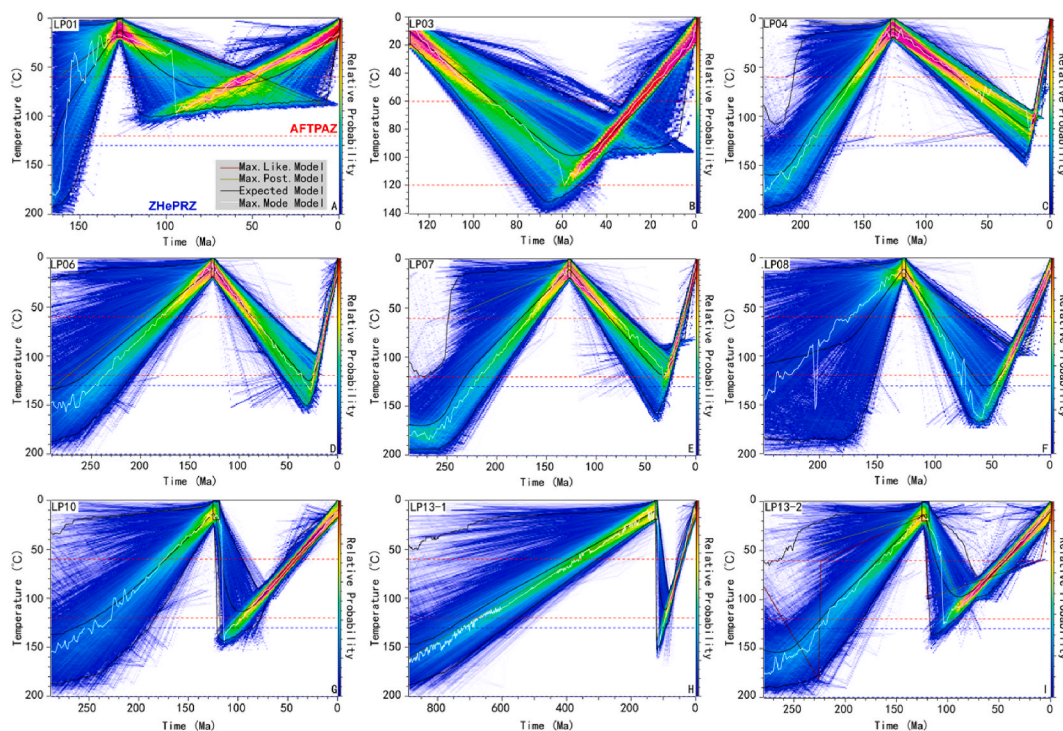ages distribution plot for CN8Ma. (D) Probability density plots (red line) and kernel density estimate (blue line) of ZHe ages for CN8Ma. Bandwidth = 50 Ma.

Fig. 4. (A)–(I) Inverse thermal history modeling for all samples (LP01, LP03, LP04, LP06, LP07, LP08, LP10, LP13-1, and LP13-2) using QTQt software for 100,000 iterations. Thin black lines represent the 95 % credible intervals for the expected model. The red dashed lines are the apatite partial annealing zone and the blue dashed lines are the zircon partial retention zone. AFTPAZ-apatite partial annealing zone. ZHePRZ-zircon partial retention zone.

followed by a cooling episode that continues to the present (Fig. 4B). This *t*-T path suggests that the Paleocene cooling corresponded to an unroofing event, with a depth of ~3 km (expected model).

Samples LP04, LP06, LP07 and LP08 are from Heshangpu Formation (K_1h) on a vertical transect, located ~20 km west of LP01 (Fig. 1). The inverse thermal models for the four aforementioned samples were constrained by our ZHe ages and published AFT data (Fig. 4C–F). These models show similar and overlapping *t*-T paths, recording cooling below ~110–150 °C at ~250-220 Ma, significantly older than the depositional age. These ages reveal cooling ages in the source regions for the Lower Cretaceous sedimentary strata. This indicates that the source regions have experienced a long-term exhumation event since the Triassic. The source materials were not transported and deposited by external forces until the Early Cretaceous period. During post-depositional processes, the Lower Cretaceous strata were continuously buried, reaching a maximum temperature of 120–130 °C at ~50-30 Ma (expected model), followed by rapid cooling through the apatite partial annealing zone to present.

The major ~250 Ma unroofing event is also recorded by sample LP10 (Fig. 4G), indicating a specific exhumation history prior to deposition. Subsequently, the expected model shows the source materials began heating from the depositional age to 100 Ma, reaching temperatures exceeding 110 °C, followed by a sustained cooling through apatite partial annealing zone, involving ~3.5 km of unroofing.

Sample LP13 represents a large-scale dispersion of apparent ZHe ages, ranging from 498 to 162.5 Ma (Table 2). Apparent ages are significantly older than depositional age, indicating not reset and recording the different thermal histories of source regions. Hence, we present inversions with two distinct populations of ZHe grain ages (Fig. 4H and I). The results closely align with those of sample LP10 (Fig. 4G), suggesting a predominantly monotonic cooling pattern prior to deposition, then reheating to maximum temperature at ~100 Ma and final cooling to surface.

In summary, our results illuminate that all samples within the Liupan Shan own significantly different thermal histories. However, they overall reveal three cooling events since the Early Cretaceous, including the Late Cretaceous, the Late Paleocene-Early Eocene, and the Late Cenozoic (Fig. 5). Additionally, our inverse results also show the maximum buried depth of our study area is less than 6–7 km at ~60 Ma, in accordance with previous paleo-depth estimates [14].

5. Discussion

5.1. Provenance analysis of the Liupan Shan group and red clay

The obtained detrital ZHe ages (except LP06-1), which are older than the depositional ages of the host strata, indicate that the samples were not buried sufficiently deep (~6–7 km) to fully reset the isotopic system since sediment deposition (Figs. 3–5). Consequently, the detrital ZHe ages may be interpreted as indicators of the exhumation history and paleogeographic environment of the source regions.

The detrital ZHe ages show a primary population grouped at ~210 Ma (Fig. 3B), corresponding to the younger age peak of detrital zircon U-Pb from the same strata in the Liupan Shan (Fig. 6A). We propose that the Late Triassic zircons of the Lower Cretaceous strata primarily originate from the Qinling Orogenic Belt. This suggestion is supported by the following evidences. First, similar age peaks of U-Pb and ZHe ages indicate that the Late Triassic zircons rapidly cooled to below 180–200 °C after crystallization (>700 °C), within a typical active margin setting [50]. Generally, the U-Pb ages obtained from detrital zircons provide the crystallization ages of zircon grains, reflecting the timing of igneous rock formation or high-grade metamorphism in the source regions [51]. The ZHe ages, on the other hand, represent the time at which the zircon grains cooled through the zircon helium partial retention zone, typically occurring
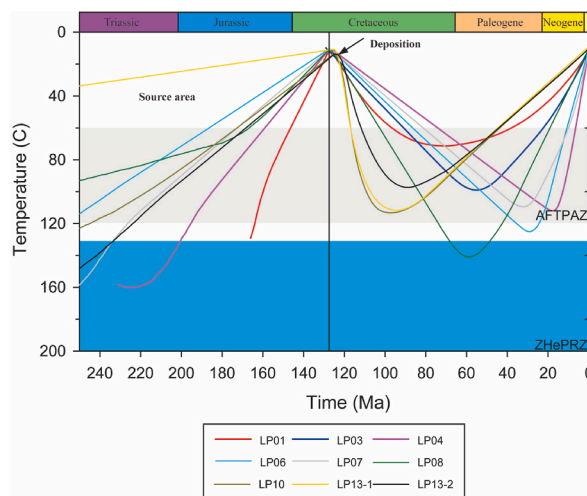

Fig. 5. The best fit time-temperature paths obtained from the expected models. Grey strip depicts apatite fission track partial annealing zone. Blue strip depicts zircon partial annealing zone. AFTPAZ-apatite partial annealing zone. ZHePRZ-zircon partial retention zone.

at temperatures of 180–200 °C. These ages are indicative of the thermal history of the source regions post-crystallization and provide insights into the timing of exhumation and erosion processes that brought these zircons to the surface before being deposited in the basin [51]. Similarities between Zircon U-Pb and ZHe ages suggest a rapid exhumation process for the pluton passing through the zircon partial retention zone during the Late Triassic, indicating a same source region [52,53]. Therefore, this rapid cooling episode should be attributed to the Late Triassic collisional orogeny. During this period, the South China Block (SCB) subducted northward, colliding with the North China Block (NCB) along the Mianlue suture zone [53–56]. This collision led to extinction of the Mianlue Ocean, crustal thickening of southern Qinling and extensive granitoid intrusions [53–56]. Second, we previously analyzed a comprehensive dataset of zircon U-Pb data around the Liupan Shan and determined that the U-Pb age spectrum closely resembles that of the Yan'an Formation from Ankou alone [13], featuring three prominent peaks at 213–218 Ma, 427–442 Ma and 892–912 Ma (Fig. 7). Consequently, we propose that these data are indicative of a unified source area. While Guo et al. [13] implied the provenance of the Yan'an Formation primarily derived from the Qilian-Qinling Orogenic Belt. Furthermore, Zhao et al. [37] integrated paleo-current directions, gravel clast compositions, and detrital zircon U-Pb data to claim that the Sanqiao and Heshangpu formations in the Liupan Shan predominantly originated from the proximal Qilian-Qinling Orogenic Belt. Their research site is about dozens of kilometers north of our study area. Third, according to the regional tectonic background, the NCB, Alxa Block, and the Qilian Orogenic Belt constitute potential source rocks for the Liupan Shan and adjacent areas (Fig. 1). However, previous studies have shown that the granites from Qilian exhibit age clusters at 420–500 Ma, 820–950 Ma, and 1100–1900 Ma. The Qinling Orogenic Belt is dominated by age peaks of 200–250 Ma, 400–520 Ma and 900–950 Ma. The U-Pb zircon ages of NCB cluster around 265 Ma, 365 Ma, 1800–2000 Ma and 2400–2800 Ma. The Alxa Block displays distinct peaks at 900–930 Ma, 1400 Ma, 1900 Ma and 2500 Ma [8,10,37,57,58]. Therefore, we unravel the zircon peak at ~210 Ma is sourced from Qinling Orogenic Belt. Fourth, the samples were primarily collected from Heshangpu and Liwaxia formations. These strata were deposited in braided river and shallow lacustrine environments, consisting of coarse sandstone and mudstone [59]. We agree that proximal sources, such as those from nearby mountains, would more likely contribute to the deposition of coarser-grained materials like conglomerates rather than fine-grained lacustrine mudstone. Fifth, previous measurements have revealed that the paleocurrents in the Early Cretaceous primarily flowed east-northeast to northwest, and that source materials were transported by these fluvial systems into the Liupan Shan and Ordos basins [59,60] (Fig. 7). The presence of
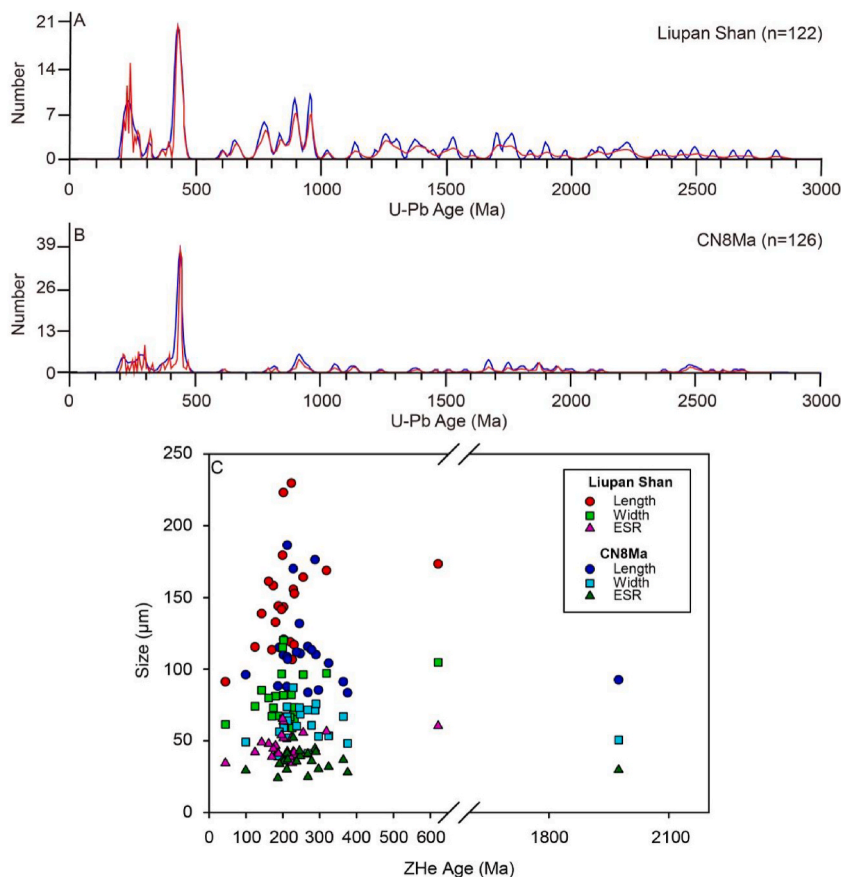

Fig. 6. A comparison between Liupan Shan and CN8Ma. (A) and (B) represent detrital zircon U-Pb ages, revised from Nie et al. [31] Red and blue lines represent probability density function (PDF) and Kernel Density Estimation (KDE) plots, respectively, and the grey rectangles are age histograms. (C) represents grain sizes. ESR: Equivalent sphere radius.
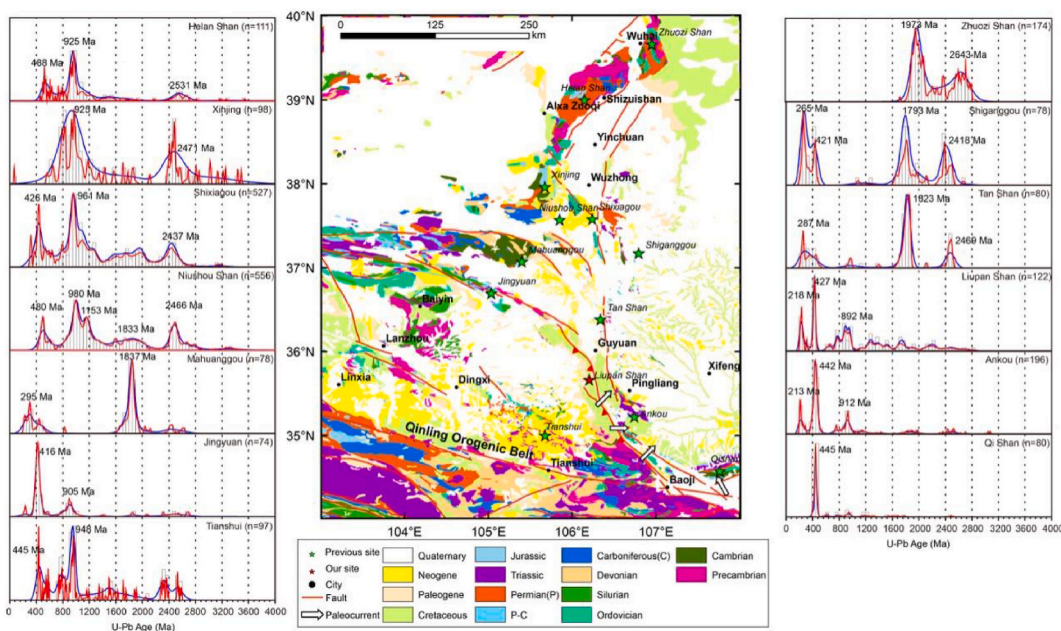
Fig. 7. Comparative detrital zircon U-Pb age distribution curves of different sites and paleocurrent directions during the early Cretaceous. The U-Pb data were derived from: Qi Shan [65], Ankou [13], Liupan Shan [31], Tan Shan [13], Shiganggou [13], Zhuozi Shan [66], Helan Shan [58], Xinjing [2], Shixiagou [2], Niushou Shan [67], Mahuangou [13], Jingyuan [2], and Tianshui [57]. The paleocurrent directions were derived from Liu [68]. Bandwidth = 50 Ma.

both coarse conglomerates and finer mudstones suggests a variable energy fluvial system with potential shifts between proximal high-energy conditions and more distal low-energy depositional environments. Sixth, the Triassic strata are extensively exposed in the Qinling Orogenic Belt (Fig. 7), potentially providing a substantial reserve of materials for the surrounding the Liupan Shan and Ordos areas. Lastly, in the Early Cretaceous, East Asian experienced widespread crustal extension, affecting areas including the Liupan Shan and Ordos Basins. This extension was associated with the rollback of the subduction zone between the continental margin and the paleo-Pacific plate, potentially leading to the post-orogenic collapse of the lower lithosphere [61]. Some suggested that the tectonic scene evolved with the Ordos Block undergoing an anticlockwise rotation, driven by the northwestward subduction of the Pacific Plate during the Early Cretaceous. This significant movement resulted in the formation of large-scale grabens, such as the Liupan Fault-Depression [35]. Alternatively, some researchers proposed that lithospheric thinning via delamination was responsible for the extension and subsequent volcanic activity in East Asia during the Early Cretaceous [62,63]. This delamination process may have reduced lithosphere thickness by over 120 km in the eastern region of the North China Craton [36,61,64]. However, regardless of the model, the extension caused the Liupan Shan area to deposit several kilometers thick of fluvial-lacustrine clastic strata around Early Cretaceous [14,23,37].

Furthermore, a previous study revealed that both the CN8Ma and Liupan Shan samples had similar zircon U-Pb age populations, ranging from 600 to 200 Ma [31] (Fig. 6A and B). Our ZHe age distributions also present the similar population between them (Fig. 3). This suggests they underwent the similar cooling event in Early Jurassic and should come from the same source region. During the Early Jurassic, the collision between SCB and NCB led to intense contraction and erosion of the Qinling and Ordos Basin, resulting in differential uplift from south to north [53–56]. Furthermore, reports indicate that the formation of the red clay, including Jiangzhangcun, Shenyu and Chaona section from west to east on the eastern margin of the Liupan Shan, occurred synchronously [19]. However, the grain size trend from coarse to fine in the base of red clay from west to east is consistent with our data (Fig. 6C), suggesting that the source of materials could be the Liupan Shan. Similarly, Zheng et al. [14] identified rapid exhumation of the Liupan Shan around ~8 Ma based on AFT data. In addition, we compared the zircon grain sizes, identifying them as a potential source of the observed date dispersion [69] (Fig. 6C). It is well-defined from Fig. 6 that the zircon grain sizes of the CN8Ma are slightly smaller than those in the Liupan Shan samples. Consequently, we postulated that the lowermost Red Clay was likely sourced from the Liupan Shan.

5.2. Paleogeographic reconstruction and exhumation history

The t-T paths of modellings captured a multi-stage phase of tectonic uplift of the Liupan Shan since the Early Cretaceous, including the Late Cretaceous, the Late Paleocene-Early Eocene, and the Late Cenozoic (Figs. 5–6).

The early cooling event originated simultaneously over widespread regions, such as Helan Shan [70], Haiyuan [18,71], Liupan Shan [18], western Qinling [72], and entire southwestern Ordos Basin [7]. Consequently, this phenomenon was interpreted as a regional exhumation event. Since the Early Cretaceous, the tectonic stress field of this study area has transitioned from nearly east-west

directed extension to northwest-southeast directed compression [21,73]. The Liupan Shan area experienced structural inversion, ending the accumulation of sediments (Figs. 4–5). Accompanied by the prolonged uplift and denudation of the Liupan Shan and Ordos Basin, it not only resulted in the non-deposition of the Late Cretaceous strata in the whole basin, but also impacted in the Alxa Block and Helan Shan [6,21,74]. This period of regional uplift, structural inversion, and extensive stratigraphic loss represented profound tectonic changes that spanned from the Eastern Pacific to Central Asia, affecting the structural domains of Central-East Asia. It signified a major transition in the Late Cretaceous geodynamic environment of Eastern China around 100 Ma, marking the completion of the transformation from the paleo-Pacific Plate to its current configuration. This marked the termination of the Yanshan Movement, which resulted from the adjustment of plate interactions in Asia and adjacent paleo-Pacific and Siberian plates, following the closure of the Tethys Ocean [75].

The second episode was almost synchronous with India-Eurasia collision [76,77]. However, it remains a puzzle how the synchronous tectonic deformation influences the Liupan Shan at the NE Tibetan Plateau. He et al. [78,79] suggested this synchronous tectonic event should be best explained by an upper crust-floating model, where deformation caused by collision and upper crustal thickening rapidly transferred to the NE Tibetan Plateau [80], rather than the stepwise rise and growth model [77] or lower crustal channel flow model [81]. When the collision between Indian and Eurasian plates occurred, the upper crust of the Tibetan Plateau rapidly ascended and transmitted the compressive stress and deformation northeastward to the NE Tibetan Plateau via a rigid block. This activation of former sutures and deep faults led to the uplift of inter-block ranges, forming new thrust-fold systems [44,80,82]. Consequently, the Liupan Shan experienced a rapid exhumation during this period.

Furthermore, the Late Cenozoic uplift event played a key role in the tectonic evolution of the NE Tibetan Plateau, although this phase remained highly controversial. In the Haiyuan-Liupan Shan area, Zheng et al. [14] suggested that rapid cooling and erosion initiated at ~8 Ma. Lin et al. [17] advocated the latest deformation episode of Haiyuan-Liupan Shan commenced in the Early Miocene, enhancing at ~9.5 Ma or in the Quaternary. Nonetheless, Wang et al. [83] revealed the enhanced sediment accumulation starting at ~10.5 Ma, based on the magnetostratigraphic in the Sikouzi section. This result is compatible with our previous simulated result [23]. Wang et al. [84] indicated that the drastic northeastern thrusting along the Haiyuan Fault took place between 15 Ma and 9 Ma, causing the rapid uplift of the fault, as evidenced by AFT and seismic reflection data. Peng et al. [71] suggested that the initial cooling of the Haiyuan Fault began at ~22-13 Ma, followed by rapid cooling during the Late Cenozoic. However, in other regions of the NE Tibetan Plateau, previous researches indicated that the north Qilianshan experienced intense fault activity during 20-10 Ma [85,86], west Qinling at ~18 Ma [87], right-lateral movement along the Elashan and Riyueshan faults between 13 Ma and 6 Ma [88], thrust faulting of the Qinghai Nan Shan at ~ 6 Ma [89], Laji Shan at ~22 Ma and Jishi Shan at 13 Ma [88], Gonghe Nan Shan between 10 Ma and 7 Ma [90]. Additionally, the basins like Guide and Linxia also reflected accelerated deformation and uplift of the NE Tibetan Plateau between 8 Ma and 6 Ma [91,92]. Collectively, these findings suggest that the uplift and deformation of the NE Tibetan Plateau spanned the entire Miocene period. During this period, the NE Tibetan Plateau underwent drastic east-west tectonic strain [15,21], consistent with the present-day crustal deformation recorded by GPS [93]. However, its propagation was asynchronous and heterogeneous, as evidenced by the aforementioned tectonic events. Wu et al. [15] proposed that the tectonic strain resulted from the far-field effect of the collision between Indian and Eurasian plates. Under the far-field influence, the northeastward expansion of the plateau was driven by a series of thrusting and strike-slip movements [77]. This dynamic was halted by the rigid Ordos Block [15], resulting in the formation of a steeper thrust wedge along the northeastern margin of the Tibetan Plateau [94].

6. Conclusions

In this work, our new detrital ZHe data, combined with corresponding thermal history modeling, provide crucial insights into the paleogeographic environment and exhumation history of the Liupan Shan. The conclusions are as follows.

(1) The detrital ZHe ages from Lower Cretaceous strata were older than the depositional ages of the host strata and had not been reset since their deposition, constraining maximum burial depths of less than 6–7 km at ~60 Ma.
(2) The source of Cretaceous materials from Liupan Shan was likely the Qinling Orogenic Belt, and the base red clay of Chaona probably originated from Liupan Shan.
(3) The Liupan Shan experienced at least three stages of tectonic events since the Early Cretaceous, including the Late Cretaceous, the Late Paleocene-Early Eocene, and the Late Cenozoic. The first tectonic event may be contacted with adjustment in plate interactions around the basin. The second event, a cooling phase, was triggered by the initial collision between India and Eurasian plates, rapidly affecting the NE Tibetan Plateau. The final episode was in response to stepwise rise and outward growth of the Tibetan Plateau.

Funding

Data availability statement

All data used can be obtained in the article.

CRediT authorship contribution statement

Declaration of competing interest

The authors declare no competing interests.

Acknowledgments

References

[1] C. Liu, H. Zhao, J. Wang, D. Zhang, M. Yang, Temporo-spatial coordinates of evolution of the Ordos Basin and its mineralization responses, Acta Geol. Sin. 82 (2008) 1229–1243, https://doi.org/10.1111/j.1755-6724.2008.tb00725.x.

[2] P. Guo, C. Liu, J. Wang, Y. Deng, S. Tyrrell, Detrital zircon geochronology of the Jurassic strata in the western Ordos Basin, North China: constraints on the provenance and its tectonic implication, Geol. J. 53 (2018) 1482–1499, https://doi.org/10.1002/gj.2968.

[3] B.J. Darby, B.D. Ritts, Mesozoic contractional deformation in the middle of the Asian tectonic collage: the intraplate Western Ordos fold–thrust belt, China, Earth Planet Sci. Lett. 205 (2002) 13–24, https://doi.org/10.1016/S0012-821X(02)01026-9.

[4] Z. Huang, Z. Ren, L. Gao, Evidence from detrital zircon and apatite fission track for tectonic evolution since Cretaceous in southeastern margin of Ordos basin, Chin. J. Geophys. 59 (2016) 3753–3764 (in Chinese).

[5] Z. Ren, Thermal history of Ordos Basin assessed by apatite fission track analysis, Chin. J. Geophys. 38 (1995) 339–349 (in Chinese).

[6] H. Zhao, C. Liu, Y. Yao, F. Wang, Y. Yin, Differential uplift in the west margin of Ordos Basin since Mesozoic from the fission track evidence, J. NW Univ. 37 (2007) 470–474 (in Chinese).

[7] Q. Yu, Z. Ren, R. Li, L. Chung, N. Tao, J. Cui, B. Wang, K. Qi, A. Khaled, Cooling history of the southwestern Ordos Basin (northern China) since late jurassic: insights from thermochronology and geothermometry, J. Asian Earth Sci. 219 (2021) 104895, https://doi.org/10.1016/j.jseaes.2021.104895.

[8] J. Sun, Y. Dong, Triassic tectonic interactions between the Alxa massif and Ordos Basin: evidence from integrated provenance analyses on sandstones, north China, J. Asian Earth Sci. 169 (2019) 162–181, https://doi.org/10.1016/j.jseaes.2018.08.002.

[9] J. Jia, W. Yin, N. Qiu, G. Wang, L. Ma, Y. Liu, N. Liu, Z.Q. Chen, Migration and accumulation of crude oil in Upper Triassic tight sand reservoirs on the southwest margin of Ordos Basin, Central China: a case study of the Honghe Oilfield, Geol. J. 53 (2018) 2280–2300, https://doi.org/10.1002/gj.3065.

[10] X. Xie, Provenance and sediment dispersal of the triassic yanchang formation, southwest Ordos Basin, China, and its implications, Sediment. Geol. 335 (2016) 1–16, https://doi.org/10.1016/j.sedgeo.2015.12.016.

[11] K. Lei, C. Liu, L. Zhang, B. Wu, X. Cun, L. Sun, Element geochemical characteristics of the Jurassic mudstones in the Northern Ordos Basin: implications for tracing sediment sources and paleoenvironment restoration, Acta Sedimentol. Sin. 35 (2017) 621–636, https://doi.org/10.14027/j.cnki.cjxb.2017.03.019 (in Chinese).

[12] W. Liu, M. Qin, F. Qi, S. Xiao, Z. Wang, Analysis on the Meso-Neozoic subsidence and uplift history of the periphery of Ordos basin using apatite fission track, Uranium Geol. 24 (2008) 221–232 (in Chinese).

[13] P. Guo, C. Liu, J. Wang, Y. Deng, G. Mao, W. Wang, Detrital-zircon geochronology of the Jurassic coal-bearing strata in the western Ordos Basin, North China: evidences for multi-cycle sedimentation, Geosci. Front. 9 (2018) 1725–1743, https://doi.org/10.1016/j.gsf.2017.11.003.

[14] D. Zheng, P.-Z. Zhang, J. Wan, D. Yuan, C. Li, G. Yin, G. Zhang, Z. Wang, W. Min, J. Chen, Rapid exhumation at ~8 Ma on the Liupan Shan thrust fault from apatite fission-track thermochronology: implications for growth of the northeastern Tibetan Plateau margin, Earth Planet Sci. Lett. 248 (2006) 198–208, https://doi.org/10.1016/j.epsl.2006.05.023.

[15] J. Wu, L. Guo, S. Xiong, S. Yang, Z. Tang, C. Jin, X. Yang, N. Gu, C. Li, J. Cui, New magnetic constraints on early-middle Miocene uplift of the liupan Shan, northeastern margin of the Tibetan plateau, G-cubed 20 (2019) 1340–1357, https://doi.org/10.1029/2018gc007944.

[16] A.R. Duvall, M.K. Clark, E. Kirby, K.A. Farley, W.H. Craddock, C. Li, D.-Y. Yuan, Low-temperature thermochronometry along the kunlun and haiyuan faults, NE Tibetan plateau: evidence for kinematic change during late-stage orogenesis, Tectonics 32 (2013) 1190–1211, https://doi.org/10.1002/tect.20072.

[17] X. Lin, H. Chen, K.-H. Wyrwoll, X. Cheng, Commencing uplift of the liupan Shan since 9.5 Ma: evidences from the Sikouzi section at its east side, J. Asian Earth Sci. 37 (2010) 350–360, https://doi.org/10.1016/j.jseaes.2009.09.005.

[18] X. Lin, H. Chen, K.-H. Wyrwoll, G.E. Batt, L. Liao, J. Xiao, The uplift history of the Haiyuan-Liupan Shan region northeast of the Present Tibetan Plateau: integrated constraint from stratigraphy and thermochronology, J. Geol. 119 (2011) 372–393, https://doi.org/10.1086/660190.

[19] Y. Song, X. Fang, J. Li, Z. An, X. Miao, The late cenozoic uplift of the liupan Shan, China, Sci. China Ser. D-Earth Sci. 44 (2001) 176–184, https://doi.org/10.1007/BF02911985.

[20] G. Ding, J. Chen, Q. Tian, X. Shen, C. Xing, K. Wei, Active faults and magnitudes of left-lateral displacement along the northern margin of the Tibetan Plateau, Tectonophysics 380 (2004) 243–260, https://doi.org/10.1016/j.tecto.2003.09.022.

[21] W. Shi, Y. Zhang, Y. Ma, G. Liu, L. Wu, Formation and modification history of the Liupanshan basin on the southwestern margin of the Ordos block and tectonic stress field evolution, Chin. Geol. 33 (2006) 1066–1074 (in Chinese).

[22] P. Zhang, B.C. Burchfiel, P. Molnar, W. Zhang, D. Jiao, Q. Deng, Y. Wang, L. Royden, F. Song, Amount and style of late cenozoic deformation in the liupan Shan area, ningxia autonomous region, China, Tectonics 10 (1991) 1111–1129, https://doi.org/10.1029/90TC02686.

[23] F. Liu, S. Cai, Quantifying the long-term slip rate of Liupan Shan thrust fault through the low-temperature thermochronology, Geol. J. (2022), https://doi.org/10.1002/gj.4587.

[24] eitao Wang, D. Zheng, J. Pang, Provenancial tracing for the Cenozoic Sikouzi section in the northeastern margin of the Tibetan Plateau and its tectonic implications, Acta Geol. Sin. 87 (2013) 1551–1569 (in Chinese).

[25] M. Bernet, C. Spiegel, Detrital thermochronology : provenance analysis, exhumation, and landscape evolution of mountain belts, Special Paper of the Geological Society of America 378 (2004).

[26] A. Bruner, A.L. Leier, D.L. Barbeau, A. Pullen, M.K. Fidler, B. Stubbins, Detrital zircon provenance and transport pathways of Pleistocene-Holocene eolian sediment in the Pampean Plains, Argentina, Geol. Soc. Am. Bull. 135 (2023) 435–448, https://doi.org/10.1130/B36267.1.

[27] Y. Ma, Z. Yang, D. He, X. Shi, B. Zhou, J. You, D. Ju, Y. Dong, Polyphase exhumation of the east Kunlun Orogenic Belt: evidence from modern river detrital zircon and apatite fission track dating, Lithosphere 2023 (2024), https://doi.org/10.2113/2023/lithosphere_2023_259.

[28] G. Bhattacharya, D.M. Robinson, D.A. Orme, (U-Th)/He thermochronology of the Indus Group, Ladakh, northwest India: is Neogene cooling a continental-scale thermal event in the India-Asia collision zone? Lithosphere 2021 (2021) 3321949 https://doi.org/10.2113/2021/3321949.

[29] W. Zhang, K. Min, S.E. Bryan, D.A. Foster, C.R. Fielding, C. Allen, A. Kerrison, Multiple post-depositional thermal events in the Drummond Basin, Australia: evidence from apatite and zircon (U-Th)/He thermochronology, Tectonophysics 767 (2019), https://doi.org/10.1016/j.tecto.2019.06.016.

[30] J. Yuan, Y. Liu, W. Li, L. Jiang, S. Yuan, S. Li, Reconstruction of the early-middle Jurassic source-to-sink system in the western Qaidam Basin (North Tibet): constraints from zircon U-Pb ages of Jurassic sediments and granites, J. Asian Earth Sci. 232 (2022) 105164, https://doi.org/10.1016/j.jseaes.2022.105164.

[31] J. Nie, W. Peng, A. Möller, Y. Song, D.F. Stockli, T. Stevens, B.K. Horton, S. Liu, A. Bird, J. Oalmann, H. Gong, X. Fang, Provenance of the upper miocene–pliocene red clay deposits of the Chinese loess plateau, Earth Planet Sci. Lett. 407 (2014) 35–47, https://doi.org/10.1016/j.epsl.2014.09.026.

[32] M. He, W. Zhang, B. Wang, H. Zheng, Provenance differentiation and earth surface process of the Mu Us sandy land constrained by detrital zircon U–Pb dating, Prog. Earth Planet. Sci. 10 (2023) 63, https://doi.org/10.1186/s40645-023-00596-6.

[33] W. Li, Y. Dong, A. Guo, X. Liu, D. Zhou, Chronology and tectonic significance of cenozoic faults in the liupanshan arcuate tectonic belt at the northeastern margin of the qinghai–tibet plateau, J. Asian Earth Sci. 73 (2013) 103–113, https://doi.org/10.1016/j.jseaes.2013.04.026.

[34] Y. Dong, S. Sun, M. Santosh, B. Hui, J. Sun, F. Zhang, B. Cheng, Z. Yang, X. Shi, D. He, L. Yang, C. Cheng, X. Liu, X. Zhou, W. Wang, N. Qi, Cross orogenic belts in Central China: implications for the tectonic and paleogeographic evolution of the east Asian continental collage, Gondwana Res. 109 (2022) 18–88, https://doi.org/10.1016/j.gr.2022.04.012.

[35] Y. Zhang, W. Shi, C. Liao, B. Hu, Fault kinematic analysis and change in late Mesozoic tectonic stress regimes in the peripheral zones of the Ordos Basin, North China, Acta Geol. Sin. 80 (2006) 639–647 (in Chinese).

[36] Y. Zhang, S. Dong, Y. Zhao, T. Zhang, Jurassic tectonics of North China: a synthetic view, Acta Geol. Sin. 82 (2008) 310–316 (in Chinese).

[37] X. Zhao, C. Liu, J. Wang, W. Luo, F. Du, L. Ma, Provenance analyses of Lower Cretaceous strata in the Liupanshan Basin: from paleocurrents indicators, conglomerate clast compositions, and zircon U-Pb geochronology, J. Earth Sci. 31 (2020) 757–771, https://doi.org/10.1007/s12583-020-1324-8.

[38] W. Wang, P. Zhang, C.N. Garzione, C. Liu, Z. Zhang, J. Pang, Y. Wang, D. Zheng, W. Zheng, H. Zhang, Pulsed Rise and Growth of the Tibetan Plateau to its Northern Margin since Ca. 30 Ma, vol. 119, Proceedings of the National Academy of Sciences, 2022 e2120364119, https://doi.org/10.1073/pnas.2120364119.

[39] X. Jin, W. Cao, Study on Cretaceous stratum system in Liupanshan region in Ningxia and its environment changes, Ningxia Eng. Technol. 5 (2006) 1–3 (in Chinese).

[40] P.W. Reiners, T.L. Spell, S. Nicolescu, K.A. Zanetti, Zircon (U-Th)/He thermochronometry: He diffusion and comparisons with 40 Ar/39 Ar dating, Geochem. Cosmochim. Acta 68 (2004) 1857–1887, https://doi.org/10.1016/j.gca.2003.10.021.

[41] M.R. Wolfe, D.F. Stockli, Zircon (U–Th)/He thermochronometry in the KTB drill hole, Germany, and its implications for bulk He diffusion kinetics in zircon, Earth Planet Sci. Lett. 295 (2010) 69–82, https://doi.org/10.1016/j.epsl.2010.03.025.

[42] K.A. Farley, R.A. Wolf, L.T. Silver, The effects of long alpha-stopping distances on (U-Th)/He ages, Geochem. Cosmochim. Acta 60 (1996) 4223–4229, https://doi.org/10.1016/S0016-7037(96)00193-7.

[43] R.M. Flowers, K.A. Farley, R.A. Ketcham, A reporting protocol for thermochronologic modeling illustrated with data from the Grand Canyon, Earth Planet Sci. Lett. 432 (2015) 425–435, https://doi.org/10.1016/j.epsl.2015.09.053.

[44] M. Jolivet, M. Brunel, D. Seward, Z. Xu, J. Yang, F. Roger, P. Tapponnier, J. Malavieille, N. Arnaud, C. Wu, Mesozoic and Cenozoic tectonics of the northern edge of the Tibetan plateau: fission-track constraints, Tectonophysics 343 (2001) 111–134, https://doi.org/10.1016/s0040-1951(01)00196-2.

[45] R.A. Ketcham, A. Carter, R.A. Donelick, J. Barbarand, A.J. Hurford, Improved modeling of fission-track annealing in apatite, Am. Mineral. 92 (2007) 799–810, https://doi.org/10.2138/am.2007.2281.

[46] B. Pan, Q. Li, X. Hu, H. Geng, Z. Liu, S. Jiang, W. Yuan, Cretaceous and Cenozoic cooling history of the eastern Qilian Shan, north-eastern margin of the Tibetan Plateau: evidence from apatite fission-track analysis, Terra. Nova 25 (2013) 431–438, https://doi.org/10.1111/ter.12052.

[47] K. Gallagher, Transdimensional inverse thermal history modeling for quantitative thermochronology, J. Geophys. Res. Solid Earth 117 (2012), https://doi.org/10.1029/2011JB008825.

[48] Y. Song, L. Qian, Late Cretaceous-Cenozoic tectonic uplift of the Liupan Shan: evidences from new apatite fission track, Acta Geol. Sin. 87 (2013) 215.

[49] P. Vermeesch, On the visualisation of detrital age distributions, Chem. Geol. 312–313 (2012) 190–194, https://doi.org/10.1016/j.chemgeo.2012.04.021.

[50] R. Spikings, G. Simpson, Rock uplift and exhumation of continental margins by the collision, accretion, and subduction of buoyant and topographically prominent oceanic crust, Tectonics 33 (2014) 635–655, https://doi.org/10.1002/2013TC003425.

[51] P.W. Reiners, R.W. Carlson, P.R. Renne, K.M. Cooper, D.E. Granger, N.M. McLean, B. Schoene, Geochronology and Thermochronology, Wiley, Hoboken, 2018.

[52] K. Cao, P.H. Leloup, G. Wang, W. Liu, G. Mahéo, T. Shen, Y. Xu, P. Sorrel, K. Zhang, Thrusting, exhumation, and basin fill on the western margin of the South China block during the India-Asia collision, Geol. Soc. Am. Bull. (2020), https://doi.org/10.1130/b35349.1.

[53] Y. Dong, G. Zhang, F. Neubauer, X. Liu, J. Genser, C. Hauzenberger, Tectonic evolution of the Qinling orogen, China: review and synthesis, J. Asian Earth Sci. 41 (2011) 213–237, https://doi.org/10.1016/j.jseaes.2011.03.002.

[54] Y. Dong, M. Santosh, Tectonic architecture and multiple orogeny of the qinling orogenic belt, Central China, Gondwana Res. 29 (2016) 1–40, https://doi.org/10.1016/j.gr.2015.06.009.

[55] Q.-R. Meng, G.-W. Zhang, Timing of collision of the North and south China blocks: controversy and reconciliation, Geology 27 (1999), https://doi.org/10.1130/0091-7613(1999)027<0123:Tocotn>2.3.Co;2.

[56] Q.-R. Meng, G.-W. Zhang, Geologic framework and tectonic evolution of the Qinling orogen, central China, Tectonophysics 323 (2000) 183–196, https://doi.org/10.1016/S0040-1951(00)00106-2.

[57] X. Pei, Z. Li, R. Li, L. Pei, C. Liu, J. Gao, F. Wei, LA-ICP-MS U-Pb ages of detrital zircons from the meta-detrital rocks of the Early Palaeozoic Huluhe Group in eastern part of Qilian orogenic belt: constraints of material source and sedimentary age, Earth Sci. Front. 19 (2012) 205–224.

[58] J. Zhang, J. Li, J. Liu, Y. Li, J. Qu, Q. Feng, The relationship between the Alxa block and the North China Plate during the early paleozoic: new information from the middle ordovician detrial zircon ages in the eastern Alxa block, Acta Petrol. Sin. 28 (2012) 2912–2934 (in Chinese).

[59] A. Ning, Depositional Evolution of Cretaceous Basin in Liupanshan Area, Northwest University Master's Thesis, 2017.

[60] J. Wang, Reconstruction of the Early Cretaceous Basin and its Evolution in Southwest Ordos, Northwest University Master's Thesis, 2007.

[61] S. Dong, Y. Zhang, F. Zhang, J. Cui, X. Chen, S. Zhang, L. Miao, J. Li, W. Shi, Z. Li, S. Huang, H. Li, Late jurassic–early cretaceous continental convergence and intracontinental orogenesis in East Asia: a synthesis of the yanshan revolution, J. Asian Earth Sci. 114 (2015) 750–770, https://doi.org/10.1016/j.jseaes.2015.08.011.

[62] J.-H. Zhang, W.-C. Ge, F.-Y. Wu, S.A. Wilde, J.-H. Yang, X.-M. Liu, Large-scale early cretaceous volcanic events in the northern great xing'an range, northeastern China, Lithos 102 (2008) 138–157, https://doi.org/10.1016/j.lithos.2007.08.011.

[63] W. Lin, M. Faure, Y. Chen, W. Ji, F. Wang, L. Wu, N. Charles, J. Wang, Q. Wang, Late Mesozoic compressional to extensional tectonics in the Yiwulüshan massif, NE China and its bearing on the evolution of the Yinshan–Yanshan orogenic belt, Gondwana Res. 23 (2013) 54–77, https://doi.org/10.1016/j.gr.2012.02.013.

[64] J. Zheng, W.L. Griffin, S.Y. O'Reilly, J. Yang, T. Li, M. Zhang, R.Y. Zhang, J.G. Liou, Mineral chemistry of peridotites from paleozoic, mesozoic and cenozoic lithosphere: constraints on mantle evolution beneath eastern China, J. Petrol. 47 (2006) 2233–2256, https://doi.org/10.1093/petrology/egl042.

[65] F. Yang, G. Chen, Q. Chen, C. Ding, L. Gao, P. Lei, W. Zhang, X. Shi, M. Tong, U-Pb dating of detrital zircon from Upper Ordovician Pingliang Formation in southwest margin of the Ordos Basin and provenance analysis, Geol. Rev. 61 (2015) 172–182 (in Chinese).

[66] B.J. Darby, G. Gehrels, Detrital zircon reference for the North China block, J. Asian Earth Sci. 26 (2006) 637–648, https://doi.org/10.1016/j.jseaes.2004.12.005.

[67] W. Yuan, Z. Yang, The Alashan Terrane was not part of North China by the Late Devonian: evidence from detrital zircon U–Pb geochronology and Hf isotopes, Gondwana Res. 27 (2015) 1270–1282, https://doi.org/10.1016/j.gr.2013.12.009.

[68] J. Liu, The Early Cretaceous Deposit and Tectonic Evolution of Liupanshan Basin, Doctor, Lanzhou University, 2010.

[69] W.R. Guenthner, P.W. Reiners, Y. Tian, Interpreting date–eU correlations in zircon (U-Th)/He datasets: a case study from the Longmen Shan, China, Earth Planet Sci. Lett. 403 (2014) 328–339, https://doi.org/10.1016/j.epsl.2014.06.050.

[70] J. Ma, D. He, Meso-Cenozoic tectonic events in the Helanshan Tectonic Belt and its adjacent areas: constraints from unconformity and fission track data, Acta Petrol. Sin. 35 (2019) 1121–1142 (in Chinese).

[71] H. Peng, J. Wang, C. Liu, S. Zhang, M. Zattin, N. Wu, Q. Feng, Thermochronological constraints on the Meso-Cenozoic tectonic evolution of the Haiyuan-Liupanshan region, northeastern Tibetan Plateau, J. Asian Earth Sci. 183 (2019), https://doi.org/10.1016/j.jseaes.2019.103966.

[72] S. Wang, Uplift History in the Southwest Margin of Liupan Shan, Mater, Northwest University, 2004.

[73] S. Dong, Y. Zhang, C. Long, Z. Yang, Q. Ji, T. Wang, J. Hu, X. Chen, Jurassic tectonic revolution in China and new interpretation of the "Yanshan Movement,", Acta Geologica Sinica - English Edition 82 (2007) 334–347, https://doi.org/10.1111/j.1755-6724.2008.tb00583.x.

[74] X. Zhao, C. Liu, J. Wang, Y. Zhao, Mesozoic geological events and its evolution sequence of the northern North-South tectonic belt, China, Geol. Rev. 64 (2018) 1324–1338 (in Chinese).

[75] C. Liu, Z. Hongge, G. Xiaojun, Y. Leping, Z. Junfeng, X. An, Space-time coordinate of the evolution and reformation and mineralization response in Ordos Basin, Acta Geol. Sin. 80 (2006) 617–638 (in Chinese).

[76] A. Yin, T.M. Harrison, Geologic evolution of the himalayan-Tibetan orogen, Annu. Rev. Earth Planet Sci. 28 (2000) 211–280, https://doi.org/10.1146/annurev. earth.28.1.211.

[77] P. Tapponnier, X. Zhiqin, F. Roger, B. Meyer, N. Arnaud, G. Wittlinger, Y. Jingsui, Oblique stepwise rise and growth of the Tibet plateau, Science 294 (2001) 1671–1677, https://doi.org/10.1126/science.105978.

[78] P. He, C. Song, Y. Wang, L. Chen, R. Bo, Cenozoic exhumation in the Qilian Shan, northeastern Tibetan Plateau: evidence from detrital fission track thermochronology in the Jiuquan Basin, J. Geophys. Res. Solid Earth 122 (2017) 6910–6927, https://doi.org/10.1002/2017JB014216.

[79] P. He, C. Song, Y. Wang, Q. Meng, L. Chen, L. Yao, R. Huang, W. Feng, S. Chen, Cenozoic deformation history of the Qilian Shan (northeastern Tibetan Plateau) constrained by detrital apatite fission-track thermochronology in the northeastern Qaidam Basin, Tectonophysics 749 (2018) 1–11, https://doi.org/10.1016/j. tecto.2018.10.017.

[80] X. Fang, D. Liu, C. Song, S. Dai, Q. Meng, Oligocene Slow and Miocene–Quaternary Rapid Deformation and Uplift of the Yumu Shan and North Qilian Shan: Evidence from High-Resolution Magnetostratigraphy and Tectonosedimentology, vol. 373, 2013, pp. 149–171, https://doi.org/10.1144/SP373.5. SP.

[81] M.K. Clark, L.H. Royden, Topographic ooze: building the eastern margin of Tibet by lower crustal flow, Geology 28 (2000) 703–706, https://doi.org/10.1130/0091-7613(2000)28<703:TOBTEM>2.0.CO;2.

[82] K.E. Dayem, P. Molnar, M.K. Clark, G.A. Houseman, Far-field lithospheric deformation in Tibet during continental collision, Tectonics 28 (2009), https://doi.org/10.1029/2008TC002344 n/a-n/a.

[83] W. Wang, P.-Z. Zhang, E. Kirby, L.-H. Wang, G.-L. Zhang, D.-W. Zheng, C.-Z. Chai, A revised chronology for Tertiary sedimentation in the Sikouzi basin: implications for the tectonic evolution of the northeastern corner of the Tibetan Plateau, Tectonophysics 505 (2011) 100–114, https://doi.org/10.1016/j. tecto.2011.04.006.

[84] W. Wang, P. Zhang, D. Zheng, J. Pang, Late Cenozoic tectonic deformation of the Haiyuan fault zone in the northeastern margin of the Tibetan Plateau, Earth Sci. Front. 21 (2014) 266–274, https://doi.org/10.13745/j.esf.2014.04.027.

[85] A.D. George, S.J. Marshallsea, K.H. Wyrwoll, C. Jie, Y. Lu, Miocene cooling in the northern Qilian Shan, northeastern margin of the Tibetan Plateau, revealed by apatite fission-track and vitrinite-reflectance analysis, Geology 29 (2001) 939, https://doi.org/10.1130/0091-7613(2001)029<0939:MCITNQ>2.0.CO;2.

[86] D.W. Zheng, M.K. Clark, P.Z. Zhang, W.J. Zheng, K.A. Farley, Erosion, fault initiation and topographic growth of the North Qilian Shan (northern Tibetan Plateau), Geosphere 6 (2010) 937–941, https://doi.org/10.1130/GES00523.1.

[87] M.K. Clark, K.A. Farley, D. Zheng, Z. Wang, A.R. Duvall, Early Cenozoic faulting of the northern Tibetan Plateau margin from apatite (U–Th)/He ages, Earth Planet Sci. Lett. 296 (2010) 78–88, https://doi.org/10.1016/j.epsl.2010.04.051.

[88] D.-Y. Yuan, J.-D. Champagnac, W.-P. Ge, P. Molnar, P.-Z. Zhang, W.-J. Zheng, H.-P. Zhang, X.-W. Liu, Late Quaternary right-lateral slip rates of faults adjacent to the lake Qinghai, northeastern margin of the Tibetan Plateau, Geol. Soc. Am. Bull. 123 (2011) 2016–2030, https://doi.org/10.1130/b30315.1.

[89] H.-P. Zhang, W.H. Craddock, R.O. Lease, W. Wang, D.-Y. Yuan, P.-Z. Zhang, P. Molnar, D.-W. Zheng, W.-J. Zheng, Magnetostratigraphy of the Neogene Chaka basin and its implications for mountain building processes in the north-eastern Tibetan Plateau, Basin Res. 24 (2012) 31–50, https://doi.org/10.1111/j.1365-2117.2011.00512.x.

[90] W. Craddock, E. Kirby, H. Zhang, Late Miocene–Pliocene range growth in the interior of the northeastern Tibetan Plateau, Lithosphere 3 (2011) 420–438, https://doi.org/10.1130/l159.1.

[91] X. Fang, C. Garzione, R. Van der Voo, J. Li, M. Fan, Flexural subsidence by 29 Ma on the NE edge of tibet from the magnetostratigraphy of Linxia basin, China, Earth Planet Sci. Lett. 210 (2003) 545–560, https://doi.org/10.1016/s0012-821x(03)00142-0.

[92] X. Fang, M. Yan, R. Van der Voo, D.K. Rea, C. Song, J.M. Parés, J. Gao, J. Nie, S. Dai, Late cenozoic deformation and uplift of the NE Tibetan plateau: evidence from high-resolution magnetostratigraphy of the Guide basin, Qinghai province, China, Geol. Soc. Am. Bull. 117 (2005) 1208–1225, https://doi.org/10.1130/b25727.1.

[93] Q. Wang, P.-Z. Zhang, J.T. Freymueller, R. Bilham, K.M. Larson, X. Lai, X. You, Z. Niu, J. Wu, Y. Li, J. Liu, Z. Yang, Q. Chen, Present-day crustal deformation in China constrained by global positioning system measurements, Science 294 (2001) 574, https://doi.org/10.1126/science.1063647.

[94] Z. Jin, D. Cunningham, C. Hongyi, Sedimentary characteristics of cenozoic strata in central-southern ningxia, NW China: implications for the evolution of the NE Qinghai–Tibetan plateau, J. Asian Earth Sci. 39 (2010) 740–759, https://doi.org/10.1016/j.jseaes.2010.05.008.